



GNSS mobile road dam surveying for TanDEM-X correction to improve the database for floodwater modeling in northern Namibia

Robert Arendt¹ · Leona Faulstich¹ · Robert Jüpner² · André Assmann³ · Joachim Lengricht⁴ · Frank Kavishe⁴ · Achim Schulte¹

Received: 27 September 2019 / Accepted: 11 June 2020 / Published online: 28 June 2020
© The Author(s) 2020

Abstract

The aim of this study is the improvement of the TanDEM-X elevation model for future floodwater modeling by implementing surveyed road dams and the use of filter algorithms. Modern satellite systems like TanDEM-X deliver high-resolution images with a high vertical and horizontal accuracy. Nevertheless, regarding special usage they sometimes reach their limits in documenting important features that are smaller than the grid size. Especially in the context of 2D-hydrodynamic flood modelling, the features that influence the runoff processes, e.g. road dams and culverts, have to be included for precise calculations. To fulfil the objective, the main road dams were surveyed, especially those that are blocking the flood water flowing from south Angola to the Etosha Pan in northern Namibia. First, a Leica GS 16 Sensor was installed on the roof of a car recording position data in real time while driving on the road dams in the Cuvelai Basin. In total, 532 km of road dams have been investigated during 4 days while driving at a top speed of 80 km/h. Due to the long driving distances, the daily regular adjustment of the base station would have been necessary but logistically not possible. Moreover, the lack of reference stations made a RTK and Network-RTK solution likewise impossible. For that reasons, the Leica *SmartLink* function was used. This method is not dependent on classic reference stations next to the GNSS sensor but instead works with geostationary satellites sending correction data in real time. The surveyed road dam elevation data have a vertical accuracy of 4.3 cm up to 10 cm. These precise measurements contribute to rectifying the TanDEM-X elevation data and thus improve the surface runoff network for the future floodwater model and should enhance the floodwater prediction for the Cuvelai Basin.

Keywords Mobile mapping · TanDEM-X · GNSS · Precise point positioning · SmartLink · Cuvelai · Iishana · Namibia

Introduction

This study is part of a broader research project in northern Namibia concerning the topics of floods and droughts and their effects on water quality in the Iishana region. Regarding floods, ongoing investigations are made to understand the hydrological system characterized by ephemeral Iishana. These net-like distributed pans may fill with water during the rainy season and inundate leading to large floods that negatively affect the Iishana region and its inhabitants. Consequences include the loss of lives and high economic losses.

Up to now, a synoptic flood forecast system is only available for the entire African continent, produced by the National Oceanic and Atmospheric Administration and its Climate Prediction Center. Detailed flood routing and prediction systems are neither available at a regional level, nor for the study area. Nevertheless, efforts have been made to prevent susceptible areas from floods: for

✉ Robert Arendt
robert.arendt@fu-berlin.de

¹ Institute of Geographical Sciences, Applied Physical Geography - Environmental Hydrology and Resource Management, Freie Universität Berlin, Malteser Strasse 74-100, 12249 Berlin, Germany

² Department of Civil Engineering, Hydraulic Engineering and Water Management, Technical University of Kaiserslautern, Paul-Ehrlich-Strasse 14-482, 67663 Kaiserslautern, Germany

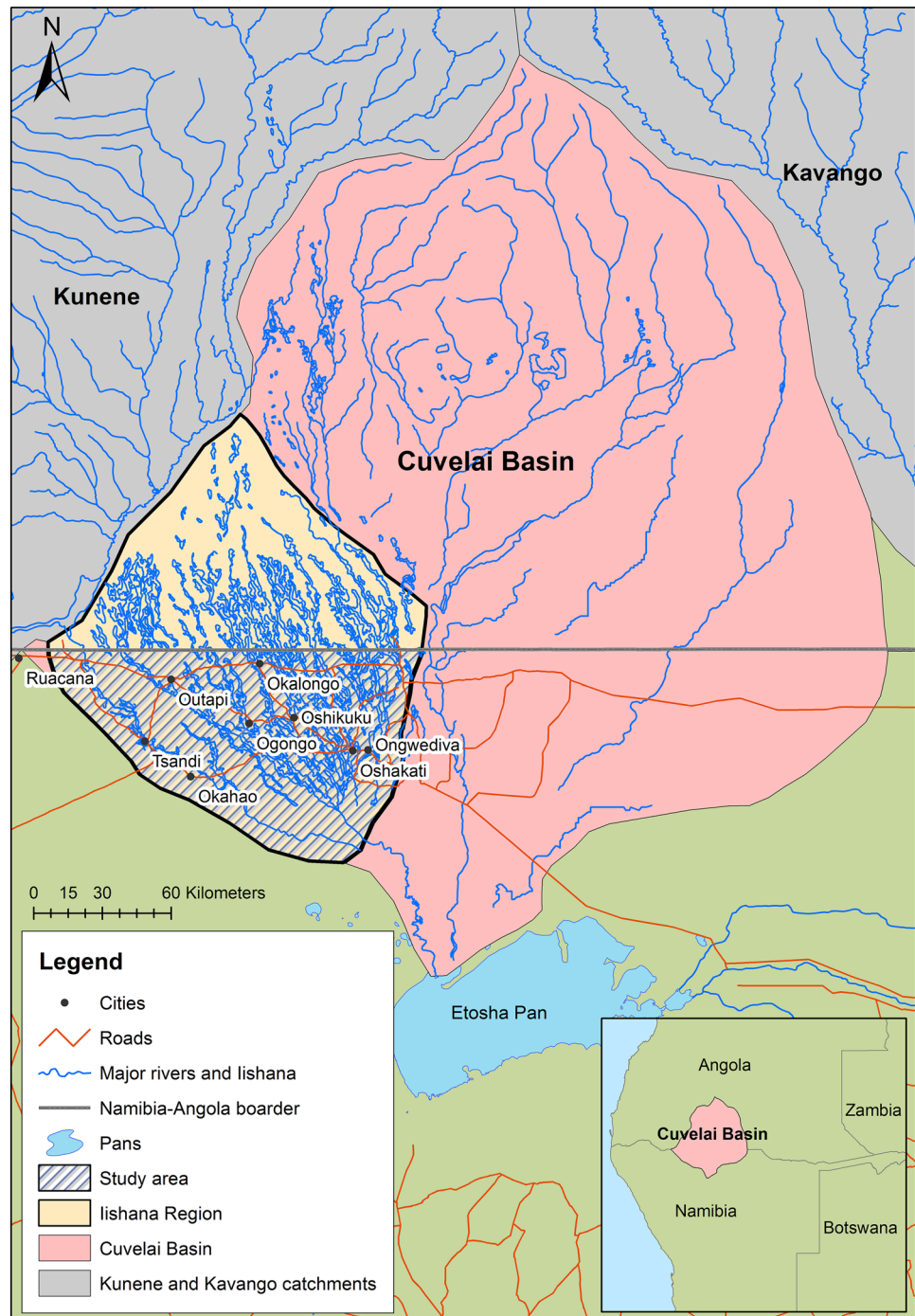
³ Geomer GmbH, Im Breitspiel 11b, 69126 Heidelberg, Germany

⁴ Faculty of Engineering and Information Technology, Department of Civil and Environmental Engineering, University of Namibia, José Eduardo Dos Santos Campus, P.O. Box 3624, Ongwediva, Namibia

example, the Namibian Early Flood Warning System, which was a sensor web-based pilot project starting in 2008. However, due to the large costs the project was not founded until the end (Mandl et al. 2012) and no longer exists. Further work has been done by Skakun et al. (2012), who extracted the maximum flood extents from satellite images for flood risk assessment. In addition, Awadallah and Tabet (2015) estimated flood extents via remote sensing data. Goormans et al. (2015) set up the

first hydrological and hydrodynamic model for the Iishana region. They focused on the city region of Oshakati and modeled the effect of a dyke, which was planned by the Ministry of Regional and Local Government, Housing and Rural Development—Oshakati Town Council in 2012 (Bethune et al. 2012) and was in some parts realized. Nevertheless, it still does not cover the whole Iishana region. For this reason, the aim is to develop a 2D-hydrodynamic flood model covering the whole Iishana area (Fig. 1). The

Fig. 1 Overview of the Cuvelai Basin and the study area of the Iishana region (source: Faulstich et al. (2018), database: UN-OCHAROSA (2018) and Digital Atlas of Namibia (2002), edited by Robert Arendt)



objective is to provide flood risk maps as well as routable flood paths. Finally, retaining-measures will be suggested and the flood model will contribute to an early warning system in the context of a broader flood risk management plan. Therefore, the model requires many input parameters like data on land use, hydrology, topography and others.

This paper focuses on the topography in the study area and discusses the digital elevation model and its improvement in accuracy for flood model calculations in a further step by correcting TanDEM-X elevation data via GNSS data. Therefore, this study is less about the detailed approach of GNSS physics itself and more about the application and combination of GNSS techniques for enhancing database for further flood modeling.

Today's modern satellites provide high-resolution images and have a high vertical and horizontal accuracy. For example, the TanDEM-X mission which delivers a digital elevation model for the whole planet with a horizontal accuracy of around 12 m and in vertical up to 2 m at least (Rizzoli et al. 2017). From the hydrological point of view, this is a great improvement to former resolutions like 20 m horizontal and 16 m to 10 m vertical accuracies of the Shuttle Radar Topography Mission (Smith 2003; Mukul et al. 2017). These advancements are important for experts modelling in the field of floods, creating more exact flood risk maps and improving the results of flood models. It becomes clear that accuracy is a factor of certainty, even more so if model results are later used for flood forecasts.

To enhance the vertical accuracy of the entire DEM, different filter algorithms have been used. Moreover, water surface interferences have been corrected by masking out (Wendleder et al. 2013) and using interpolation procedures. With these methods, natural and anthropogenic hydrological obstacles, like parts of vegetation and water-induced interferences or buildings, could be equalized. Anthropogenic obstacles, in this specific case road dams (Fig. 2), have been surveyed in real time by a GNSS sensor. These road dams play a significant role in the Iishana region, which is characterized by a very low relief where almost every small sink or elevation influences the flow dynamic. Using the GNSS sensor to localize specific points precisely on the ground has been a common method used in industry and science for years (Bisnath et al. 2003; Arroyo et al. 2005; Gao et al. 2005; Knoop et al. 2017). If using a differential system an accuracy in a millimeter range is readily achieved. However, differential GNS-systems always need a base station in a certain range, otherwise the accuracy decreases dramatically up to a loss of connection. For example, the Leica GS16 System works properly up to 1 km in differential mode. If this is not wide enough for a certain use, it is possible to use the common Real-Time Kinematic (RTK) or Network-RTK mode, like other GNS-Systems. Both RTK

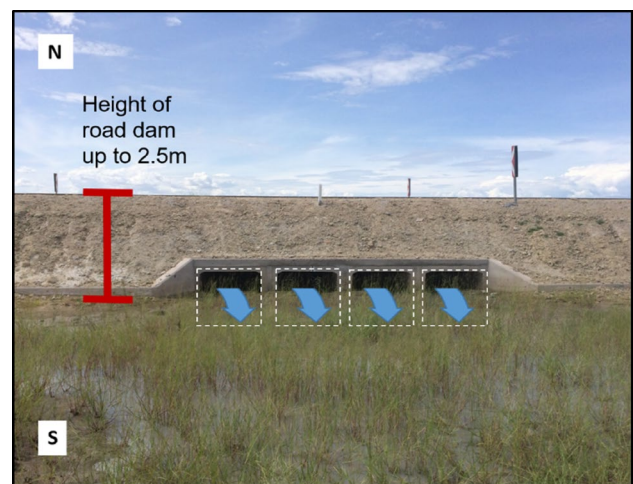


Fig. 2 High road dam crossing an Oshana in transverse direction. Water flows from north to south through the culverts. The culverts (white dotted boxes) are heavily sedimented. (Photo and editing: Robert Arendt 2018)

solutions receive their correction data either from a single or even from a network of reference stations a few kilometers nearby. These systems use UHF/VHF radio signals or mobile phone networks to send their correction data to the GNSS sensor. This technique is very well known in vehicle navigation and in cases of precision farming (Knoop et al. 2017; Shrivathsa and Panjwani 2017; Skog and Handel 2009; Gebbers and Adamchuk 2010; Dixon 2006). The accuracy of (Network-) RTK generated GNSS data differs in a sub-centimeter range. In terms of precision farming, the vehicles are driving slowly with a maximum speed of 11 km/h. Even here, their work range is limited by the availability of reference stations and their application is expensive (Perez-Ruiz and Upadhyaya 2012). Moreover, potential connection losses lead to reduced accuracy up to a meter range.

To become more independent, the Satellite Based Augmentation System (SBAS) was formerly invented for the offshore industry in the early 1990s (Barboux 2000). Offshore platforms need to be constructed precisely, although they are usually located far away from the coast. In these remote areas, no reference stations are available. This method nowadays is called Real-Time Precise Point Positioning. In this case, the GNSS system receives the correction data directly from a geostationary satellite, which makes it applicable all around the world (Skog and Handel 2009; Perez-Ruiz and Upadhyaya 2012).

In this study, a Leica GS16 Sensor was installed on the roof of a car. While driving along the road dams with a maximum speed of 80 km/h, elevation surveys were automatically corrected in real time via the commercial Leica *SmartLink* function within a centimeter of accuracy. After

the days of recording, the data were corrected by eliminating outliers and redundant measurements. In a next step, the elevation data were implemented into the post processed TanDEM-dataset for further hydrodynamic calculations.

Materials and methods

Study area

Namibia's climate is strongly influenced by the cold Benguela current along the west coast of South Africa leading to arid and semi-arid conditions. Determined by the Inter-tropical Convergence Zone (ITCZ), rainy season runs from October to April and dry season from May to September.

A hydrologically diverse region therein is the trans-boundary Cuvelai Basin, which itself is bounded to the north by the Kunene River and Okavango River in Angola and by the Etosha Pan on the south in Namibia. The western edge is defined by the city of Ruacana and the eastern edge lies between the cities of Okongo and Mpungu Vlei. The Cuvelai Basin is divided into eight major drainage zones (Mendelsohn et al. 2013).

In this case, the study area is part of the Iishana region, consisting of the Western Oshana Zone and the Central Oshana Zone (Cunningham et al. 1992). Reduced to the Namibian state territory, it is marked to the north by the Namibian-Angolan boarder. The western edge is marked by the city of Ruacana and in the east by the city of Oshakati (Faulstich et al. 2018) (Fig. 1). The annual amount of precipitation is between 350 up to 550 mm increasing from west to east and is characterized by high rainfall variability. The potential evaporation rises in the same direction from 2.600 to 3.200 mm (Mendelsohn et al. 2013; Persendt et al. 2015). The terrain is about 1.100–1.200 m a.s.l. and has a very flat slope ranging from 0.5 to 1.0 m/km (Mendelsohn et al. 2013). The surface hydrology is featured by a large ephemeral river system and is affected by irregular floods during rainy seasons (Sakakun et al. 2012; Kuliwoye 2010; Kundzewicz et al. 2014; Shifidi 2014). These low slope, net-like troughs and sinks run in a northwesterly to southeasterly direction. The water depth during floods is about 1–7 m. Namibia gains most of its rainfall in the study area. The soils are profitable for agricultural use. These circumstances lead to the fact that around 40% of Namibia's population lives in the northern region (Mendelsohn et al. 2013). Nevertheless, next to near-surface Aeolian and fluvial sediments of clay deposits, lime and silicate crusts, produce low infiltration capacities and high surface runoff (Hüser et al. 2001; Nguno and Angombe 2011; Goudie and Viles 2015). These facts result in widespread flooding during rainy season. While most of the surface water comes from the

Angolan side of the Iishana region, floods are intensified by local convective rain events. Fatal floods in the recent past have occurred in 2008, 2009, 2010, 2011 and 2013. The large inundations affected human lives, caused huge damage to health, extensive damage to property and technical infrastructures like roads, bridges and dams (Mandl et al. 2012; Skakun et al. 2012; Awdalla and Tabet 2015; Persendt et al. 2015; Bischofberger et al. 2015; Filali-Meknassi and Ouarda 2014; Mufeti 2013).

The hydrodynamic model

In this particular study, the specific flood prediction problem is a combination of multiple factors. The large catchment of about 10.000 km² and the TanDEM-X raster resolution of 12.5 m needs a model that is able to handle the amount of data in an adequate time. Moreover, the model needs the ability to incorporate culverts and bridges. Furthermore, the relief is very flat (slope ranging from 0.5 to 1.0 m/km), the flow speeds of floods is low (Cunningham et al. 1992) and even low obstacles can substantially change the flow behavior instantly. Nonetheless, at the same time, these areas affected by floods should be recorded as precisely as possible. Therefore, the hydrodynamic model 'FloodArea' will be used in a future step to calculate the runoff, flow concentration, flow velocity, backwater situations and inundation depth for variable time steps. 'FloodArea' is based on a simplified hydraulic approach including hydrodynamic calculations for the simulation of large areas with high spatial resolution (< 1 m) (Fritsch et al. 2016). Successful applications have been made in large-scale simulations of catchments sized up to 3.000 km² in Germany (Assmann et al. 2013). As mentioned above, the hydrodynamic calculation itself will not be discussed in this work. Further literature regarding 'FloodArea' is reported in Anders et al. (2016); Assman et al. (2013) and Fritsch et al. (2016).

Road dams and culverts

According to the cited TanDEM-X accuracy, small objects like road dams are not displayed. These road dams are elongated artificial fillings of earth material or rock on which a road runs. A road dam is designed to elevate and thus overcome geomorphological and topographical obstacles and thus has a landscape-shaping effect. It must not be compared to flood protection dams, because its construction is altogether simpler and not suitable as a flood protection measure. The road embankment has no overflows or other auxiliary structures, with the exception of culverts. Its structure is not designed for the lateral pressure of large water masses and additionally hinders natural flow processes and drainage channels.

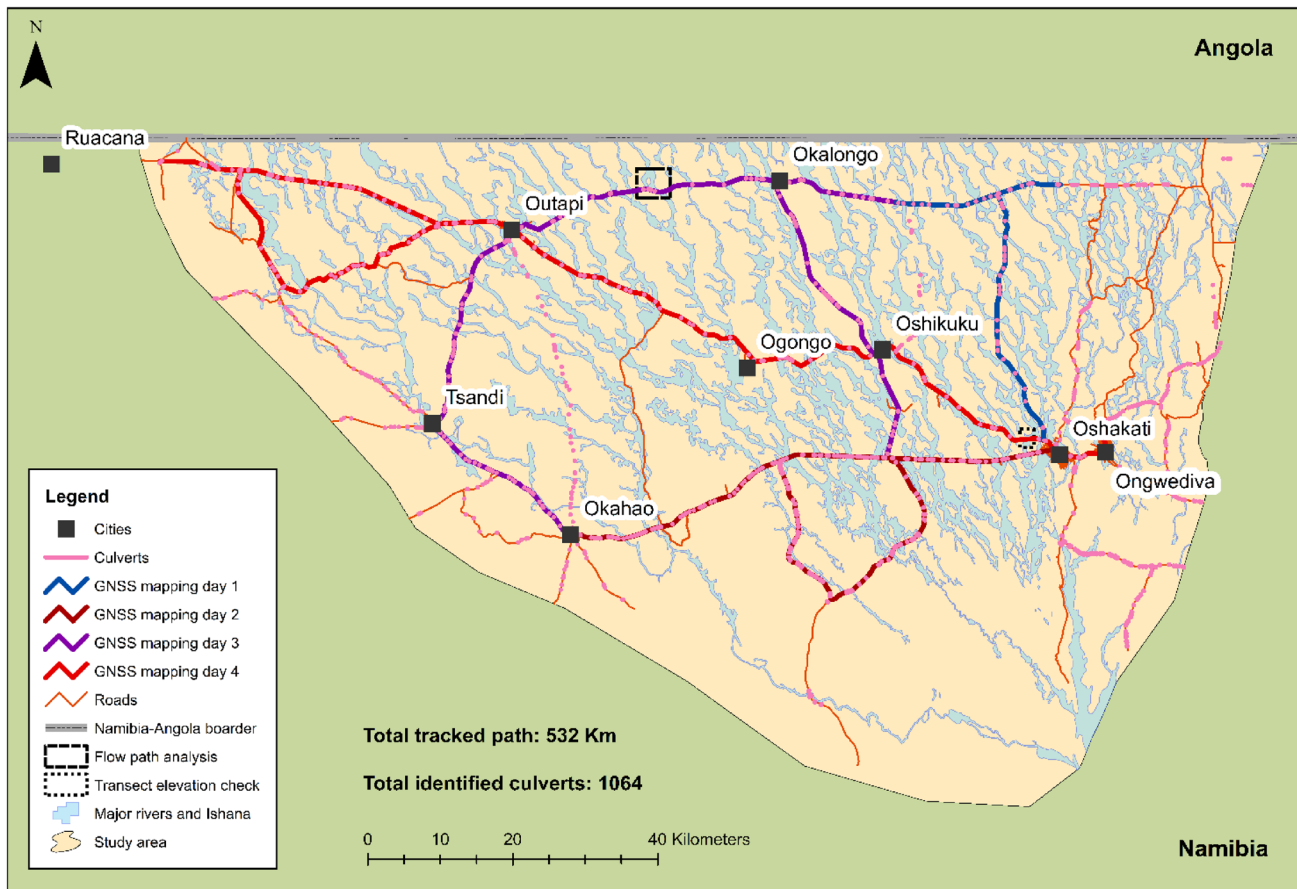


Fig. 3 Map including the surveyed road dams and culverts (source: Faulstich et al. (2018), database: UN-OCHAROSA (2018) and Digital Atlas of Namibia (2002), edited and mapping by Robert Arendt)

Most of the roads in the study area are almost orthogonally affected by the Iishana system (Fig. 3), and the major cities are connected by the shortest route and lowest construction costs. During most of the year (normal rainy season and dry season), this infrastructure is not negatively affected by water. In the case of an “Efundja”, a local name for a major flood, they become vulnerable to overspilling and erosion (Mendelsohn et al. 2013).

On one hand, these road dams change the flow directions and hinder flow processes, which have to be taken into account by the hydrodynamic model. There is a water build-up and settlement structures in this area are more affected by the floods. Of course, during this time, these important infrastructure facilities cannot be used. As an example for the benefit of measuring and implementing these road dams into the DEM, the divergence in elevation between the TanDEM-X raw data and the GNSS measured values shows differences ranging from 0.125 up to 1.955 m (“GNSS and TanDEM-X cross validation” section).

On the other hand, culverts and bridges have to be included and incorporated into the model. The consideration

of small structures like low walls or road dams is crucial to analyze flow paths and assess the influence of flow velocity. (Fritsch et al. 2016). Therefore, over 1000 culverts and bridges were mapped via google earth satellite images and have been cross-validated during the field trip via a hand hold Garmin e-Trex GPS (Fig. 3).

A high-resolution DEM including significant obstacles is essential for the accuracy in modeling surface runoff. An accurate DEM increases the predictive capacity of the flood model in terms of a better identification of main flow paths and local sinks, the locations of high flow depths and accelerated flow velocities (Fritsch et al. 2016). The exact magnitude of the advantage cannot yet be described until the model has been run, but can be assumed as enhanced as the flow path analysis shows in the results (“Corrected TanDEM-X” section). This analysis was done three times with different pre-settings. The first flow path calculation considered the TanDEM-X raw data set by using just the ‘Fill’ function in advance. Otherwise, there would be no flow path calculation possible. The second calculation also used the filter algorithms (“DEM pre-processing and

correction" section). The third calculation included more than 1000 culverts and bridges (Fig. 3). The flow path calculations were done according to the work of Persendt and Gomez (2016) and used the D8 algorithm as a simple approach for a validation process.

GNSS and real-time kinematic precise point positioning

The surveying of positions with the Global Navigation Satellite System (GNSS) is a common method for personal navigation and is ubiquitous. It is omnipresent, whether while driving with cars or for navigation during outdoor activities, in science and industrial sectors, or for surveying and lane detection (Knoop et al. 2017). Currently, few GNS Systems are available. The most prominent and first developed GNS System is the American Global Positioning System (GPS) that emerged in the 1990s (Zumberge et al. 1997). At the same time, many different positioning systems are available. The European Space Agency (ESA) developed the Galileo Program. There is the Chinese system BeiDou and the Russian system GLONASS, which have been working parallel to GPS for many years (Skog and Handel 2009; Li et al. 2015; Liu et al. 2017). GNSS positioning is the most basic technique and founded on the measurement of pseudo-range (Shrivathsa and Paniwani 2017).

Main disturbances in positioning appear in the ionosphere and the troposphere. Therefore, different methods exist to decrease these errors. One strategies is the use of an a-priori model to estimate the residual effects from measurements (Shrivathsa and Paniwani 2017). In case of ionospheric delays, only around half of it can be deleted and errors of several meters can still occur. Another strategy to improve the accuracy is to measure the delay by collecting data with a dual-frequency receiver. These devices are more expensive (Shrivathsa and Paniwani 2017; Skog and Handel 2009).

Higher accuracies can be reached by Relative Positioning with the integration of proximate static reference stations, e.g. with Network-RTK stations. With these techniques, common mode errors for GNSS receivers in a terminated area are estimated by a nearby stationary reference station that transmits the corrected information to the rover typically via UHF radio signals (Xu 2012). The common mode error increases with distance between the rover and the base station (Skog and Handel 2009). In differential mode, a pseudo-range measurement can reach accuracies within a centimeter up to millimeter dimension (Shrivathsa and Paniwani 2017). Combining the pseudo-range measurements and carrier-phase measurements improves the accuracy even more by providing unknown carrier phase cycle ambiguities and fix them to their integer value (Knoop et al. 2017; Ge et al. 2008; Teunissen and Khodabandeh 2014). Negative aspects of differential or relative GNSS positioning are the large and

costly data transfer and the need of a dense local network of reference stations in a (Network-) RTK mode (Knoop et al. 2017; Shrivathsa and Paniwani 2017).

During the last 20 years, precise point positioning (PPP) achieved powerful advancements, which significantly led to increasing accuracy. It developed from former single-frequency constellation (just GPS) to multiple GNSS constellations like GPS, GLONASS, BeiDou and Galileo (Li et al. 2015; Cai and Gao 2007; He 2015). It further enhanced from single over dual up to triple frequencies and from ambiguity-float to ambiguity-fixed solutions (Liu et al. 2018). Moreover, as a key for base station-independent work, it evolved from post-processing to real-time processing (Dixon 2006), usable in a static or even in a kinematic mode, via a globally distributed network of reference stations and geostationary satellites (Liu et al. 2018; Bisnath and Gao 2009; Kaplan and Hegarty 2005). Thus, PPP developed into a method able to measure precise point positions in a kinematic mode and correcting in real-time—real-time kinematic precise point positioning (RTKPPP) (Bisnath and Gao 2009). The main applications for RTKPPP are in the field of precision farming (Dixon 2006; Perez-Ruiz and Upadhyaya 2012) and marine constructions (Arroyo-Suarez et al. 2005).

PPP almost works like a Differential GNSS but instead of calculating the position relatively to a nearby ground or base station, it uses correction data send via a geostationary satellite. This technique provides accurate position data almost all over the globe in a decimeter, up to centimeter quality (Knoop et al. 2017; Shrivathsa and Panjwani 2017; Liu et al. 2018; Bisnath and Gao 2009; Kaplan and Hegarty 2005; Hatch et al. 2003). In a PPP system, the receiver uses the clock and orbit information of the satellite itself, and also the correction data from a relatively sparse global tracking network on the ground (Li et al. 2015). This stationary network calculates the correction for all visible satellites and the ensemble of this correction data is formatted into a binary message. This message is then sent to the Hub where it is uplinked to the geostationary satellite (Knoop et al. 2017; Shrivathsa and Panjwani 2017; Liu et al. 2018; Bisnath and Gao 2009; Kaplan and Hegarty 2005; Hatch et al. 2003). The geostationary satellite broadcasts the information to the receiving antenna on the ground (Fig. 4). The communication runs in the L-band format for GPS constellation (Skog and Handel 2009; Li et al. 2015; Kaplan and Hegarty 2005; Hatch et al. 2003). A dual-frequency receiver reduces the amount of reference stations needed to attain high accuracy (Shrivathsa and Panjwani 2017; Hatch et al. 2003). The satellite-based correction data is usually offered by commercial service providers (Liu et al. 2018; Bisnath and Gao 2009) like VERIPOS Apex/Apex²/Apex⁵, OmniSTAR G2, TERRASTAR-D, NavCom, Trimble CenterPoint RTX and SartFire. For open source use, the PPP-Wizard and RTKLIB are available (Jokinen 2014).

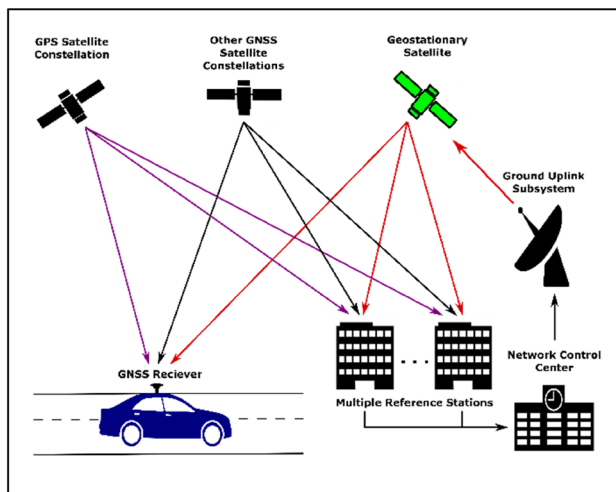


Fig. 4 Operation of real-time-kinematic precise point positioning (source: edited after NovTel Inc. (2015), modified by Robert Arendt)

Nowadays, different providers like the BKG (Bundesamt für Kartographie und Geodäsie), CNES (Centre National d'Études Spatiales), DLR (Deutsches Luft und Raumfahrtzentrum), ESA/ESOC (European Space Agency/European Space Operations Centre), GFZ (Deutsches GeoForschungsZentrum) deliver freely accessible correction data. More and detailed information regarding the topic of post-processing is discussed in Wang et al. (2018). A cutout of the globally distributed reference stations can be seen in Li et al. (2015) and are further explained in Skog and Handel (2009).

To achieve an accuracy of up to 5 cm a convergence time of 20–60 min is normally needed, depending on the actual number and geometry of visible satellites. To prevent a loss of tracking or a lock on a minimum of satellites, an open sky is needed as well as a continuously unobstructed environment (Knoop et al. 2017; Bisnath and Gao 2009). On the other hand, the use of PPP has its advantages in isolated and remote locations, expansive areas and regions where a reference station infrastructure is not generally available or is too costly (Bisnath and Gao 2009).

Sensor specifications

The Leica Viva GS16 smart antenna is a multi-frequency GNSS Sensor running together with the Leica CS20 Field Controller. Signal tracking is working with GPS (L1, L2, L2C, L5), GLONASS (L1, L2), BeiDou (B1, B2, B3 limited), Galileo (E1, E5a, E5b, Alt-BOC, E6 limited), QZSS (in future), SBAS (WAAS, EGNOS, MSAS, GAGAN) and L-band. The intern Satel M3-TR4 radio modem has 555 channels which leads to a high sensitivity and fast acquisition. The sensor can be used as a normal GNSS (absolute

point positioning), in differential modus as a base station or rover as well as in a real-time-kinematic modus (RTK) with adaptive on-the-fly satellite selection (relative positioning). The RTK single baseline performance is about $8 \text{ mm} + 1 \text{ ppm}$ horizontal and $15 \text{ mm} + 1 \text{ ppm}$ in vertical. In the Network RTK mode an accuracy of $8 \text{ mm} + 0.5 \text{ ppm}$ horizontal and $15 \text{ mm} + 0.5 \text{ ppm}$ in vertical can be reached. Post-processed data measured in a static phase with long observation time can have an accuracy of about $3 \text{ mm} + 0.1 \text{ ppm}$ horizontal and $3.5 \text{ mm} + 0.4 \text{ ppm}$ vertically. The specialty of the sensor is its commercial *SmartLink* worldwide correction service based on the *VERIPOS Apex* correction service (In this study *Apex²* service). The *SmartLink* and *SmartLink fill* function is a remote Precise Point Positioning system with an accuracy up to 3 cm in 2D. The measurement precision, accuracy and reliability is dependent on various factors like the number of available satellites, observation time, atmospheric conditions, multipath and others. The convergence time needed to gain full accuracy can take 20 up to 40 min. More general sensor information can be read in Leica GS 16 manual (Leica Geosystems AG 2018).

Using the *SmartLink* function means that permanent corrected data can be received from a geostationary satellite (RTKPPP, derived via 7 different geostationary satellites—*25E, 98 W, 143.5E, AORE, AORW, IOR, POR*) (Fig. 4). The accuracy in the commercial *SmartLink* mode is lower than in the RTK mode but it is independent of proximate reference stations and applicable all over the world. A statistical post-processing is not required because the *SmartLink* software automatically corrects the ionospheric and tropospheric delay as well as orbit and clock lags with help of the geostationary satellite information.

The geometric arrangement of the satellites, called Dilution of Precision (DOP), is given as GDOP (3 position coordinates plus clock offset in solution) and PDOP (Position of 3 coordinates) (Hurn 1989). A negative aspect of this commercial service is the stochastic black box, where the user has no option to look at the correct functional model and the proper intra- and inter-system weighting of observations behind (Kazmierski et al. 2018; Kazmierski 2018).

Further negative aspects of using commercial correction data instead of the free available data, for example of the CNES are its high costs and less accurate results against post-processed data.

However, depending on the task and its required accuracy it can make investigations less complex for the end-user.

Measurement setup and processing strategy

For mapping the road dams, the GS 16 Sensor was installed on the roof of a 4×4 car (Figs. 5, 6). The offset between the sensor and the street surface was measured with a Leica



Fig. 5 Leica GS 16 Sensor installed on the roof of a car (photo: Robert Arendt 2018)



Fig. 6 Measurement setup—Toyota Hilux with GS 16 sensor on the car roof (photo and editing: Robert Arendt 2018)

LaserDisto 8 and results in 1.93 m (Fig. 6). The sensor was connected via Bluetooth with the Leica CS20 Field-Controller in the car. This was programmed to take points automatically every 25 m or more frequently if there is an elevation change of more than 0.3 m in between that distance. The range was chosen according to the TanDEM-X digital elevation model, which has a raster resolution of 12.5 m. A higher waypoint resolution would have been possible but was not necessary because most of the time no significant elevation change was recognized in between a higher raster resolution, as previous fieldwork has shown.

The coordinate reference frame used by Apex² is ITRF2014. Due to the settings of the Field Controller CS20 it was automatically transferred into ITRF2008 and later measurements were reassigned in a geodetic format with ellipsoid and datum WGS 84, further given in Cartesian projected coordinate system UTM 33 S. Selectable satellite systems were GPS, GLONASS, Galileo and BeiDou. The

Leica *SmartLink* option was selected by activating the Augmentation System so signals from geostationary satellites and their real-time correction data could be received. As mentioned above, the used commercial function is based on the VERIPOS Apex² system that only allows the receiving of real-time correction data for GPS and GLONASS. That is why real-time correction data for BeiDou and Galileo could not be received. The quality of the received correction data is guaranteed by the ISO 17123-8. More information about the processing strategy can be read in Table 1. The satellite cut-off angle was set on 10°. A DOP limit was not determined in advance but verified in the post-evaluation.

Each of the four surveying days (Fig. 3) started and ended at the campus site of the University of Namibia in Ongwediva. Before driving commenced, the GS16 was installed on the car and a convergence time of 20 to 40 min was given until the sensor achieved a 1D accuracy of lower than 10 cm.

Due to the limitation in time and parallel projects, the focus was on the main roads and required:

1. Transverse course to the flow direction of the Iishana and
2. Security for the drivers, passengers and the car.

Therefore, some remote gravel roads lacking security had to be excluded, like the part between Okahao and Outapi, which was too dangerous to drive on. The road dams east of Oshakati and Ongwediva have been excluded, because the hydrological network is different from the western system and will not be investigated further (Fig. 3). In addition, a part of short track between Tsandi and Ruacana is ignored as the system is flowing almost parallel to the road, so that the road dam will not have any important influence on the flow

Table 1 Processing strategy

Processing mode	Real-time
Observables	Ionospheric-free linear combination code and carrier-phase measurements
Ambiguities	float
Signal frequencies	GPS: L1/L2, GLONASS: L1/L2
Inter-System weighting	VERIPOS Apex ²
Elevation cut-off angle	10°
Sampling rate	25 m and/or change in elevation > 30 cm
Troposphere delay modeling	VERIPOS Apex ²
Receiver clock	VERIPOS Apex ²
Satellite orbits and clocks	VERIPOS Apex ²
Code and phase biases	VERIPOS Apex ²
Solution type	kinematic, VERIPOS Apex ²
Correction models	VERIPOS Apex ²

Compliant to the ISO 17123-8 standard

dynamic in this part of the study area (Fig. 3). A longer track starting west of the city of Okahao leading east of Ogongo has been omitted in consequence of its flatness.

The driving speed spanned between 0 and 80 km/h. During breaks, for example at traffic lights, the speed was 0 meanwhile the speed on long straight route sections was constantly about 80 km/h. In general, the speed was adapted to the road conditions and traffic situation. Outliers like waypoints leading to parking lots have been excluded manually. Furthermore, it has to be considered that the transverse gradient of the roads, especially in wide curves, could not always be driven along the highest positions due to road traffic regulations. To improve the process of validation, data from the Namibian Roads Authority (NRA) were utilized for cross validation. Three datasets M0092, M0133, M0123 were provided.

The NRA partly measured the same roads and their heights within a distance of 500 m with the TRIMBLE R10 GNSS receiver in 2015. Likewise using a proprietary provider for real time correction in motion, they took the Trimble Continental CenterPoint RTX data. Similar to the measuring campaign of this study, they drove along the roads with a maximum speed of 80 km/h recorded in ITRF2014 coordinate reference frame, which was later converted into a WGS 84 format. They also measured while connected to the GPS and GLONASS systems. Another part in the set up was the PDOP value. If the value rose more than 0.5 m surveying ceased. Even in this investigation, post-processing was not necessarily done because of the real-time correction. The NRA could not give information that is more detailed. Nevertheless, both datasets measured nearly the same coordinates, just with another commercial device and software but still in the same mode.

Other cross validation methods, such as double and triple measurements or single point long time static measurements, have not been executed due to the lack of time in the field campaign.

The results of the two kinematic measurement campaigns of 2015 and 2018 were later compared for cross checking and to validate their deviations and similarities giving a hint of the overall reliability of the results.

The major challenge was to find coordinates that are at an equal location for further comparison. Most of the surveyed points could not be taken for validation because both campaigns measured in opposite directions and at different distances (25–500 m). Therefore, a buffer of 3 m was set around the coordinates of the 2018 campaign and intersected with the NRA data. The setting of 3 m was chosen under the condition that every pair of points had to be as close as possible for a significant comparison. Otherwise, if the buffer was set smaller almost no pairs of points were left for comparison. Finally, 18 points were

close enough to each other for further comparison imitating a double measurement at these locations.

DEM pre-processing and correction

The correction of the TanDEM-X data set took place in several steps. In step one, outliers in elevation and indifferences caused by water were sought for exclusion. Therefore, the data package of the TanDEM-X data set includes different additional information layers (Wessel 2016). In this case, the TanDEM-X Water Indication Mask was used for excluding the strong inconsistencies (Wendleder et al. 2013).

The generated holes have to be interpolated to adapt the surface to the surrounding area. This was done with the Image Analyzer in ArcGIS. Here, the mask function was used with a minimum value of 0 and a maximum value of 3034 for band 1. As a result, missing values were set to NoData. Afterwards gaps were filled with the Elevation void fill function (Short Range IDW Radius “off” and Max. Void Width “fill all”). Then, smaller sinks were filled with the standard Fill function of ArcGIS to eliminate further voids. Subsequently extreme values were reduced by a low-pass filter 3×3 (Pipaud et al. 2015). The last step is about the implementation of the GNSS records. Therein a 25 m buffer was set around the GNSS point data. Afterwards, a Kernel interpolation between the GNSS points was set in between the buffer area. Then, the new dataset was implemented by the ArcGIS function Mosaic to new raster.

Results

GNSS performance

The measurement setup could be applied on all road dams as planned. At the end, 16.590 points were taken and around 532 km of main road dams were tracked (Fig. 3). Nevertheless, in the post-evaluation of the recorded data, it became clear that points were not taken exactly every 25 m as was defined in the automatic mode. Most points were taken in a range between 25 and 27 m. Moreover, a large amount of points was taken in distances up to 49 m. Statistically, points have been collected within a mean of every 32.08 m.

Nevertheless, the overall GNSS performance shows PDOP and GDOP values within an excellent to ideal rating between 3.5 and 1.2 (Tables 2, 3) (Dutt et al. 2009; Langley 1999). It should be mentioned that the performance rating originally was invented for GPS only (Langley 1999).

In addition, the 1D, 2D and 3D coordinate quality (CQ) is also determined in a decimeter to a sub-decimeter range, where 1D describes the vertical accuracy, 2D the horizontal accuracy and 3D the spherical (vertical and horizontal) accuracy. As reported in Table 2, the range of total accuracy

Table 2 Overview of used satellites and accuracies of the recorded GNSS data

Satellites used	Day 1	Day 2	Day 3	Day 4
GPS	7–8	7–10	7	10
GLONASS	6–7	4–8	7	6
Total detected	17–21	11–20	16–17	18–19
Accuracy				
PDOP	1.4–1.7	1.2–2.1	1.2–2.9	1.3–2.8
GDOP	1.6–2.0	1.2–2.2	1.3–3.5	1.2–2.3
1DCQ [cm]	7.1–9.9	4.3–9.0	4.7–10.0	4.4–10.0
2DCQ [cm]	3.2–5.4	2.4–6.3	2.5–6.2	2.4–7.8
3DCQ [cm]	7.8–9.9	5.0–10.0	5.3–10.0	5.0–10.0

Table 3 Explanation of DOP quality, after Langley (1999) in Dutt et al. (2009)

DOP value	Rating
1	Ideal
2–4	Excellent
4–6	Good
6–8	Moderate
8–20	Fair
20–50	Poor

in the sector of 3D coordinate quality spans from 5.0 to 10.0 cm, where 10 cm was the cut off limit. Points with a lower accuracy were excluded in the post-evaluation process.

The calculated 3DCQ mean is about 7.1 cm with a standard deviation of 1.1 cm and a skewness of 0.544. The 1D and 2D coordinate quality is even better (Table 2).

GNSS and TanDEM-X cross validation

The cross-validation of the two surveying campaigns (Table 4) between Leica and Trimble shows differences in height between 0.006 and 0.585 m with a mean difference of 0.154 m and a median difference of 0.091 m. The standard deviation is about 0.160 m with a skewness of 1.386 and a variance of 0.026. The calculated RMSE is about 0.219.

Moreover, the measurements of the 2018 campaign with the Leica instrument were compared to the TanDEM-X raw data at the same positions. Obviously, the range is larger. The minimum deviation is 0.125 m and the maximum deviation is up to 1.955 m, with a mean difference of 0.418 m and a median of 0.471 m. The standard deviation is 0.973 m with a skewness of -1.138 and a variance of 0.947. The calculated RMSE is about 1.059.

Corrected TanDEM-X

The TanDEM-X Transect Elevation Check of Fig. 7 shows two different lines and a blue plain of height along a transect,

which can be found in Figs. 8, 9. The black line indicates the height of the TanDEM-X raw data set before any calculation. The red dotted line designates the same path after the correction of water interferences and the application of filtering algorithms as described before (DEM pre-processing and correction). Up to here, the topography is smoothed and represents a more realistic and natural image. Sharpe edges could be equalized and some overestimated parts (water interferences and vegetation patches) have been lowered while other underestimated parts have been raised. Until that point, the road dam is still not clearly visible.

The plain blue specifies the final corrected DEM including the surveyed road dam, which is visible also in Fig. 9. Except for the road dam where more than a meter deviation is evident, differences in a sub-meter range could be detected. As shown in Figs. 8, 9, the application of the different filter algorithms and the correction of the water-induced interferences have been successful, so the road dam is clearly visible and the high outrage peaks are eliminated.

The value of the results becomes clearer in Fig. 10. The effect of the road dams and the modifications including culverts and bridges leads to a change in flow behavior, here emphasized in a change of flow direction. The calculated flow paths change significantly between the raw TanDEM-X model and the two edited models where additional filter algorithms were applied and culverts and bridges have been included.

Discussion

Due to left hand-traffic, data points were usually collected while driving on the left side of the roads. It has to be acknowledged, that road dams are normally transversely inclined in curves. Therefore, some of the collected point data in curves are not always representing the highest part of the road dam cross section. Nevertheless, in a few parts, the attempt was made to drive the highest profile through the curves to gain the maximum height of the road dam. These circumstances led to small differences between the left and right roadsides, which theoretically has to be added to the general vertical accuracy (1DCQ).

Airfreight costs could be saved, as just one sensor was necessary instead of two and no additional equipment. Moreover, time and work force was saved, because no differential station had to be set up every 1 km nor always had to be guarded by staff. Even the long convergence time of 30–40 min at the beginning of the measurement session was no problem at all, since this time was used to prepare the daily fieldwork.

According to Langley (1999), the GDOP and PDOP values had excellent to ideal rates. This explanation of quality was formerly developed for GPS only. Even the 1D, 2D and

Table 4 Cross validation of measurements with Leica, Trimble and the TanDEM-X

Leica point ID	Height Leica [m]	Trimble point ID	Height Trimble [m]	Horizontal distance between points [m]	Absolute vertical deviation Leica and Trimble [m]	Height TanDEM-X [m]	Absolute vertical deviation Leica and TdX [m]	Statistics for vertical deviation of Leica and Trimble data	Statistics for vertical deviation of total measured points of Leica at TdX raw data position
3410	1129.933	256	1129.927	2.449	0.006	1129.423	0.510	Mean value [m]	Mean value [m]
9948	1127.953	35	1127.961	2.732	0.008	1129.241	1.288	0.154	0.418
10,968	1124.560	97	1124.576	2.955	0.016	1124.000	0.560		
7422	1125.875	47	1125.852	2.908	0.023	1126.000	0.125	Median [m]	Median [m]
3476	1128.586	260	1128.642	2.593	0.057	1129.250	0.664	0.091	0.471
9807	1128.516	26	1128.574	2.880	0.058	1127.661	0.856		
9987	1128.039	37	1127.981	2.912	0.058	1126.044	1.995	Stand. deviation [m]	Stand. deviation [m]
10,712	1125.969	82	1125.906	2.425	0.063	1126.309	0.339	0.160	0.973
10,098	1127.549	43	1127.631	2.837	0.083	1127.276	0.273		
4541	1132.345	345	1132.246	1.045	0.099	1131.327	1.018	Skewness	Skewness
10,762	1125.696	85	1125.570	2.688	0.126	1125.227	0.470	1.386	- 1.138
3080	1127.226	234	1127.087	1.594	0.139	1126.000	1.226		
10,748	1125.774	84	1125.574	2.949	0.200	1126.006	0.233	Variance	Variance
11,039	1124.491	101	1124.257	2.455	0.234	1123.000	1.491	0.026	0.947
9744	1128.929	21	1129.170	2.989	0.241	1128.019	0.910		
4628	1133.556	340	1133.891	2.300	0.335	1133.921	0.365	RMSE	RMSE
4683	1132.567	337	1133.000	1.172	0.433	1133.292	0.724	0.219	1.059
4835	1131.988	328	1132.573	3.000	0.585	1131.723	0.265		
								Min/Max [m]	Min/Max [m]
								0.006/0.585	0.125/1.955

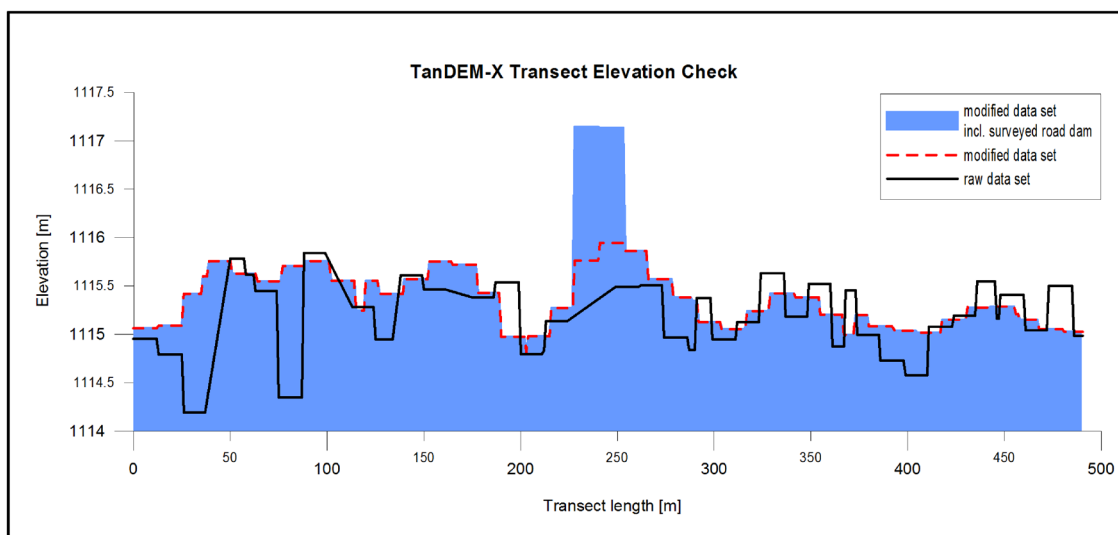


Fig. 7 TanDEM-X Transect Elevation Check (located in Figs. 3, 8 and 9)

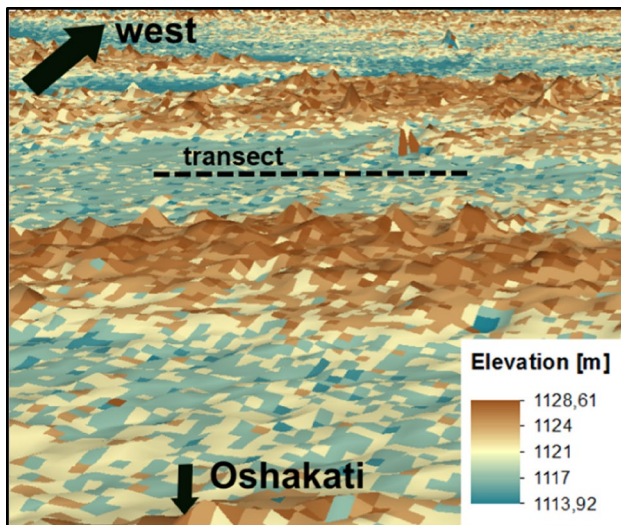


Fig. 8 TanDEM-X scene before correction. Both scenes face in a western direction with exaggeration $\times 12$ and the indication of the transect of Fig. 7 (also located in Fig. 3)

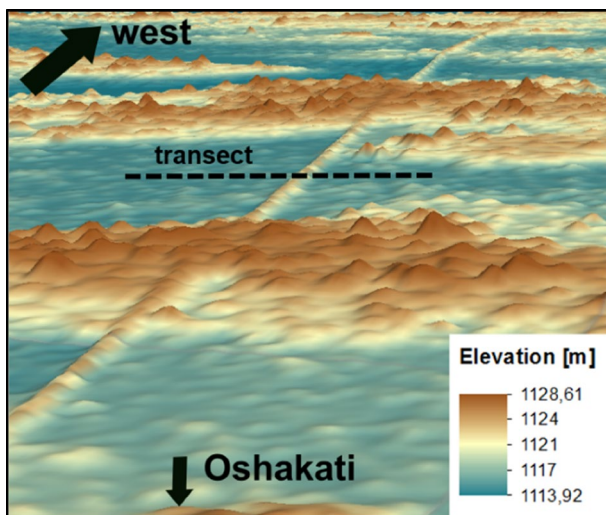


Fig. 9 TanDEM-X scene after correction. Both scenes face in a western direction with exaggeration $\times 12$ and the indication of the transect of Fig. 7 (also located in Fig. 3)

3D coordinate accuracy shows a decimeter to sub-decimeter deviation. Nonetheless, coordinates could not have been detected 100% accurately every 25 m as was planned and set in the settings. It is assumed that the top speed of 80 km/h might be too high if points information were recorded every 25 m. Regarding future measurements, either the top speed has to be limited or the record span has to be widened. First estimations indicate that it is more about velocity. Some extreme outliers can be explained by an exceeding of top speed for example, due to overtaking, and others may be caused by a longer software calculation time.

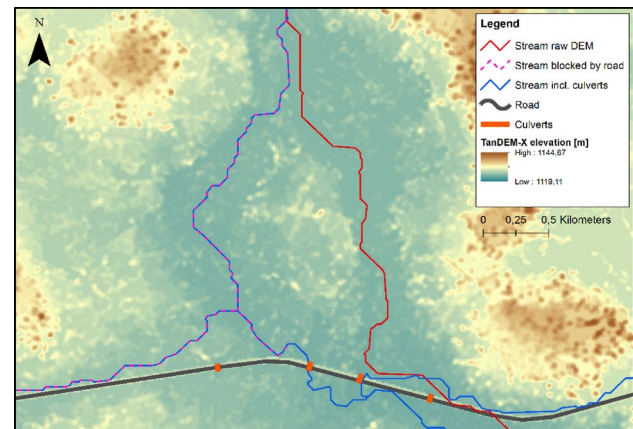


Fig. 10 Three different flow path calculations with ArcGIS illustrated in one image. Red stream definition based on the raw TanDEM-X model only used the 'Fill' function. Purple dotted Stream is calculated after the application of additional filter algorithms and the inclusion of the road dams. The blue Stream also includes the culverts and bridges. The road dams and culverts are influencing the flow dynamics

It can be assumed that multipath effects were not important, due to the sparsely vegetated and very flat landscape being only rarely interrupted by trees or buildings. Multipath effects caused by the white metal roof of the car cannot be determined nor excluded. Literature did not give any hints about necessary protection measures for roof top installed GNSS sensors, nor any numbers for multipath measurement errors.

The filter algorithm used leads to a substantial improvement. The evaluation of the transect as well as Figs. 7, 8, 9 shows that most of the interferences could be eliminated successfully and the geomorphology is obviously more perceptible. Nonetheless, the delivered water mask did not cover all water surfaces, especially very small ones sometimes were not covered. As a consequence, the low-pass filter smoothed these objects but some of them still exist as small dunes. However, regarding the work of Wendleder et al. (2013), it can be assumed that around 70% of the water bodies were detected. Further statistics regarding the used water mask are pending and have to be evaluated in a next step.

The validation of the measured data was limited due to the use of commercial real-time correction data. This caused a black-box effect in which not all data quality parameters were visible. Long-term single point measurements and double and triple measurements could not have been done due to limitation of time and parallel investigations in the field. Therefore, the only chance to get an idea of the vertical accuracy was the comparison of the data with former measured data from the Namibian Roads Authority. In this case, different systems were used but with almost the same settings,

measuring in motion with the same speed and the use of a commercial real-time correction service. Statistical analyses showed a sub-decimeter median value. Nonetheless, even for the data of the NRA individual quality values were missing due to the commercial real-time correction service used.

To achieve real-time correction data that is free of charge different providers like the CNES can be addressed for future measurements. In addition, post-processing would contribute to increased accuracy (Wang et al. 2018; Kazmierski et al. 2018; Kazmierski 2018). For example, with the new VERIPOS Apex⁵ system, receiving of correction data including BeiDou and Galileo would have been possible to increase data quality. Even with the CLK91 stream via CNES free available correction data including all 4 satellite systems could have been received (Wang et al. 2018).

To some extent, the final total estimated error in height consists of different single errors and cannot be assessed in a concluding number due to various factors: the position of the car on the street (top or down of the turn), the uncertainty of the commercial real-time correction data (partially black-box), the TanDEM-X itself (vertical/horizontal accuracy), and filter algorithms and interpolation procedures used. It becomes clear that a millimeter accuracy cannot be reached at all. Nonetheless, the aim of the work—to improve the TanDEM-X data set for further flood modelling—has been achieved.

Conclusions

The application of the different filter algorithms and the correction of the water-induced interferences have been successful, so road dams have been made clearly visible and high outrage peaks were eliminated. These modifications including culverts and bridges also lead to a change of flow directions. The automatically recoded points present excellent up to ideal GDOP and PDOP values with vertical accuracies about 4.3 cm up to 10.0 cm. The validation procedure shows huge vertical differences between GNSS measurements and the TanDEM-X raw model ranging from about 0.125 m up to 1.955 m with a median of 0.471 m. Elevation differences between two GNSS systems have shown significantly less differences in accuracy ranging between 0.006 and 0.585 m with a median of 0.091 m. These circumstances clearly illustrate the necessity of measuring smaller infrastructures for an accurate representation in the digital elevation model.

With this investigation, a scientific contribution has been made towards understanding the topographic basis of the Iishana system. Previously developed hydrological models in the Iishana region were focused on small sub-basins rather than on the entire system. The survey results reported here provide a scientific base for developing a trans-boundary

flood model in the Iishana region of Angola and Namibia which would contribute towards an innovative adaptation of water management to climate change. The potential and originality of this research project is to bridge the knowledge gaps and to contribute to the scientific base for sustainable water resource management in the region.

The results underline the significance of a preprocessing of TanDEM-X data and the importance of incorporating road dams, culverts and bridges when a high quality flood-water prediction model is sought.

Acknowledgements Open Access funding provided by Projekt DEAL. We thank the German Aerospace Centre (© DLR 2017) for their delivery and support with the TanDEM-X data (Proposal ID: DEM_HYDR1285). Further, we thank the Leica Geosystems AG for their quick and helpful technical support during our field campaign in March 2018. Moreover, we thank the "German Association for International Cooperation (GIZ) GmbH" (Windhoek, Namibia office, Prof. Dr. Heinrich Semar) for the logistical support of the field campaign in September 2017 and March 2018. We are grateful for the collaboration with the University of Namibia (Campus Ongwediva) and the Namibian Roads Authority (Windhoek, Mr. Horst Schommarz) for providing us with data. We also thank Mr. Benjamin Rommel (Freie Universitaet Berlin) for constructing the special tools for the sensor installation.

Author contributions Conceptualization: RA and AS; Methodology: RA; Software: RA and AA; Validation: RA and RJ; Formal analysis: RA, AS, RJ and LF; Investigation: RA, LF, AA and AS; Resources: JL and FK; writing—original draft preparation: RA, AS, RJ and LF; writing—review and editing: RA, LF, AS and RJ; Visualization: RA; Supervision: AS and RJ; Project administration: AS.

Funding This research was supported by the Freie Universitaet Berlin and the "Research Network for Geoscience in Berlin and Potsdam—Geo-X".

Compliance with ethical standards

Conflicts of interest The authors declare no conflict of interest.

Open Access This article is licensed under a Creative Commons Attribution 4.0 International License, which permits use, sharing, adaptation, distribution and reproduction in any medium or format, as long as you give appropriate credit to the original author(s) and the source, provide a link to the Creative Commons licence, and indicate if changes were made. The images or other third party material in this article are included in the article's Creative Commons licence, unless indicated otherwise in a credit line to the material. If material is not included in the article's Creative Commons licence and your intended use is not permitted by statutory regulation or exceeds the permitted use, you will need to obtain permission directly from the copyright holder. To view a copy of this licence, visit <http://creativecommons.org/licenses/by/4.0/>.

References

- Anders K, Assmann A, Fritsch K (2016) Prospects and requirements for an operational modelling unit in flood crisis situation, E3S Web of Conferences 7, 19002, FLOODrisk 2016, 3rd European Conference on Flood Risk Management, DOI: 10.1051/e3sconf/20160719002

- Assmann A, Jäger S, Fritsch, Brauner C (2013) Risk maps for pluvial flooding and infiltration of a flood risk management process, In: Klinj F, Scheckendiek (ed) Comprehensive flood risk management. Research for policy and practice: 189. Proceedings of the 2nd European conference on flood risk management FLOODrisk 2012, Rotterdam
- Arroyo-Suarez EN, Riley JL, Glang GF, Mabey D (2005) Evaluating a global differential GPS system for hydrographic surveying. In: Proceedings of OCEANS 2005 MTS/IEEE, OCEANS 2005 MTS/IEEE, Washington, DC, USA, 18–23 Sept, IEEE 1–7, DOI: 10.1109/OCEANS.2005.1640155
- Awadallah AG, Tabet D (2015) Estimating flooding extent at high return period for ungauged braided systems using remote sensing: a case study of Cuvelai Basin Angola. *Nat Hazards* 77(1):255–272. <https://doi.org/10.1007/s11069-015-1600-6>
- Barboux JP (2000) Navigation and Positioning Practices in the Off-shore Industry. In: B, Schürmann (ed) Proceedings of the International Symposium GEOMARK 2000 Paris France 10–12 April 2000, European Space Agency (ESA) 2000, Noordwijk, The Netherlands, ESA SP 458 49 p
- Bethune S, van der Waal B, Roberts KS (2012) Proposed flood mitigation measures for the Oshakati/Ongwediva Area, Environmental Impact Assessment (EIA), Draft Scoping Report, May 2012
- Bischofberger J, Schuldt-Baumgart N, Lenzen E (2015) Omeya ogo omwenyo—water is life, CuveWaters Report
- Bisnath S, Gao Y (2009) Current state of precise point positioning and future prospects and limitations, In: Michael G. Sideris (ed): Observing our changing earth, Proceedings of the 2007 IAG general assembly Perugia Italy July 2–13 2007 Bd, 133, Berlin Heidelberg: Springer 2009 (International Association of Geodesy Symposia vol, 133) 615–623. DOI: 10.1007/978-3-540-85426-5_71
- Bisnath S, Wells D, Dodd D (2003) Evaluation of commercial carrier phase-based WADGPS services for marine applications, In: ION GPS/GNSS 2003 Portland Oregon, 17–27
- Cai C, Gao Y (2007) Precise point positioning using combined GPS and GLONASS observations. *J GPS* 6(1):13–22. <https://doi.org/10.5081/jgps.6.1.13>
- Cunningham T, Kinahan J, Marsh A, Stuart-Williams V, Hubbard D, Kreike E, Seely M (1992) Oshanas, Sustaining people environment and development in central Owambo Namibia, ISBN 9991670904
- Digital Atlas of Namibia (2002) https://www.uni-koeln.de/sfb389/e1/download/atlas_namibia/haupt_namibia_atlas.html. Accessed 26 Oct 2016
- Dixon K (2006) StarFire: A Global SBAS for Sub-Decimeter Precise Point Positioning. Proceedings of the 19th International Technical Meeting of the Satellite Division of The Institute of Navigation (ION GNSS 2006) Fort Worth, TX, September 2006, 2286–2296
- Dutt VBSSI, Rao GSB, Rani SS, Babu SR, Goswami RG, Kumari ChU (2009) Investigation of GDOP for precise user position computation with all satellites in view and optimum four satellite configurations. *J Ind Geophys Union* 13(3):139–148
- Faulstich L, Schulte A, Arendt R, Kavishe F, Lengricht J (2018) Die Qualität der intensiv genutzten Oberflächengewässer im Cuvelai-Becken (Nord-Namibia) zum Ende der Trockenzeit 2017, In: Chiffard P, Karthe D, Möller S (eds) Geographica Augustana, Beiträge zum 49. Jahrestreffen des Arbeitskreises Hydrologie vom 23.–25. November 2017 in Göttingen, Band 26, Augsburg 2018
- Filali-Meknassi Y, Ouarda TBMJ, Wilcox C (2014) Data access availability and quality assessment for the development of a flood forecasting model for Namibia, Technical Report United Nations Educational Scientific and Cultural Organization 78 Document code: WIN/2014/IHP/01
- Fritsch K, Assmann A, Tyrna B (2016) Long-term experiences with pluvial flood risk management, E3S Web of Conferences 7, 04017 (2016), FLOODrisk 2016 -3rd European Conference on Flood Risk Management, DOI: 10.1051/e3sconf/20160704017
- Gao Y, Wojciechowski A, Chen K (2005) Airborne kinematic positioning using precise point positioning methodology. *Geomatica* 59(1):29–36
- Ge M, Gendt G, Rothacher M, Shi C, Liu J (2008) Resolution of GPS carrier-phase ambiguities in precise point positioning (PPP) with daily observations. *J Geod* 82(7):389–399. <https://doi.org/10.1007/s00190-007-0187-4>
- Gebbers R, Adamchuk VI (2010) Precision agriculture and food security. *Science (New York NY)* 327(5967):828–831. <https://doi.org/10.1126/science.1183899>
- Goormans T, van Looveren R, Mufeti P, Wynants J (2015) Building a hydrological and hydrodynamic model while facing challenges in data availability in the Oshana Region of Central Northern Namibia, E-proceedings of the 36th IAHR World Congress, 28 June–3 July 2015 The Hague, The Netherlands
- Goudie A, Viles H (2015) Landscape and landforms of Namibia, Springer Heidelberg, ISBN: 978-94-017-8020-9
- Hatch R, Sharpe TS, Galyean P (2003) StarFire: a global high accuracy differential GPS system. In: Proceeding of the 2003 National Technical Meeting of The Institute of Navigation, Anaheim CA, 562–573
- He K (2015) GNSS kinematic position and velocity determination for airborne gravimetry, PhD Thesis (Scientific Technical Report 15/04) Potsdam: Deutsches Geoforschungszentrum GFZ 158 p.
- Hüser K, Besler H, Blümel WD, Heine K, Leser H, Rust U (2001) Namibia—eine Landschaftskunde in Bildern, Edition Namibia 5, Göttingen Windhoek, 272, ISBN: 9783933117144
- Hurn J (1989) GPS: a guide to the next utility, Sunnyvale Trimble Navigation 1989. 76 p. ISBN: 10-9992537019
- Jokinen AS (2014) Enhanced ambiguity resolution and integrity monitoring methods for precise point positioning, PhD thesis at Imperial College London, Centre for Transport Studies, Department of Civil and Environmental Engineering
- Kaplan E, Hegarty C (2005) Understanding GPS principles and applications, principles and applications, 2nd ed. Norwood: Artech House 2006, 726 p. ISBN: 1580538940
- Kazmierski K (2018) Performance of absolute real-time multi-GNSS kinematic positioning. *Artif Satellites*. <https://doi.org/10.2478/arsa-2018-0007>
- Kazmierski K, Hadas T, Sosnica K (2018) Weighting of multi-GNSS observations in real-time precise point positioning. *Remote Sens* 10:84 <https://doi.org/10.3390/rs10010084>
- Knoop VL, de Bakker PF, Tiberius CCJM, van Arem B (2017) Lane determination with GPS precise point positioning. *IEEE Trans Intell Transport Syst* 18(9):2503–2513. <https://doi.org/10.1109/TITS.2016.2632751>
- Kuliwoye EK (2010) Flood Hazard Assessment by means of Remote Sensing and Spatial analyses in the Cuvelai Basin, Case Study Ohangwena Region–Northern Namibia, 2010 Master thesis Seminar Series Nr. 218
- Kundzewicz ZW, Kanae S, Seneviratne SI, Handmer J, Nicholls N, Peduzzi P, Mechler R, Bouwer LM, Arnell N, Mach K, Muir-Wood R, Brakenridge GR, Kron W, Benito G, Honda Y, Takahashi K, Sherstyukov B (2014) Flood risk and climate change: global and regional perspectives. *Hydrol Sci J* 59(1):1–28. <https://doi.org/10.1080/02626667.2013.857411>
- Langley RB (1999) Dilution of precision. *GPS World* 10(5):52–68
- Leica Geosystems AG (2018) Sensor specifications. https://leica-geosystems.com//media/Files/LeicaGeosystems/Products/Datasheets/Leica_Viva_GS16_DS.aspx?la=en&hash=EB1C7278B6E75F4ADD9E80849879557. Accessed 14 Sept 2018
- Li X, Ge M, Dai X, Ren X, Fritsche M, Wickert J, Schuh H (2015) Accuracy and reliability of multi-GNSS real-time

- precise positioning: GPS GLONASS BeiDou and Galileo. *J Geod* 89(6):607–635. <https://doi.org/10.1007/s00190-015-0802-8>
- Liu T, Yuan Y, Zhang B, Wang N, Tan B, Chen Y (2017) Multi-GNSS precise point positioning (MGPPP) using raw observations. *J Geod* 91(3):253–268. <https://doi.org/10.1007/s00190-016-0960-3>
- Liu T, Zhang B, Yuan Y, Li M (2018) Real-time precise point positioning (RTPPP) with raw observations and its application in real-time regional ionospheric VTEC modeling. *J Geod* 92(11):1267–1283. <https://doi.org/10.1007/s00190-018-1118-2>
- Mandl D, Frye S, Sohlberg R, Cappelaere P, Handy M, Grossman R (2012) The Namibia early flood warning system a CEOS pilot project. In: IEEE international geoscience and remote sensing symposium (IGARSS) 2012, 22–27 July 2012 Munich Germany Annual IEEE Computer Conference, IEEE, Piscataway, NJ, 3521–3524. DOI: 10.1109/IGARSS.2012.6350660
- Mendelsohn J, Jarvis A, Robertson T (2013) A profile and atlas of the Cuvelai-Etoshia Basin, 170 p. RAISON & Gondwana Collection Windhoek Namibia, ISBN 978-99916-780-7-8
- Mufeti P, Rientjes THM, Mabande P, Maathuis BHP (2013) Application of a satellite based rainfall-runoff model: a case study of the trans boundary Cuvelai Basin in Southern Africa, ESA living planet symposium proceedings of the conference 9–13 September 2013, Edinburgh, UK, ESA SP-722, 2–13 p 82
- Mukul M, Srivastava V, Jade S, Mukul M (2017) Uncertainties in the shuttle radar topography mission (SRTM) heights: insights from the Indian Himalaya and Peninsula. *Sci Rep* 7:41672. <https://doi.org/10.1038/srep41672>
- Nguno A, Angombe M (2011) Mapping of clay and salt pans in northern Namibia using remote sensing and field spectral techniques. 35th Canadian Symposium on Remote Sensing, pp. 2–4
- NovAtel Inc (2015) An introduction to GNSS, GPS GLONASS BeiDou Galileo and other Global Navigation Satellite Systems, Second Edition, Canada (2015), ISBN: 978-0-9813754-0-3
- Perez-Ruiz M, Upadhyaya SK (2012) GNSS in precision agricultural operations. In: Fouzia Elbahhar (ed) New approach of indoor and outdoor localization systems, InTech. <https://doi.org/10.5772/50448>
- Persendt FC, Gomez C (2016) Assessment of drainage network extractions in a low-relief area of the Cuvelai Basin (Namibia) from multiple sources: LiDAR, topographic maps, and digital aerial orthophotographs. *Geomorphology* 260(2016):32–50. <https://doi.org/10.1016/j.geomorph.2016.06.047>
- Persendt FC, Gomez C, Zawar-Reza P (2015) Identifying hydro-meteorological events from precipitation extremes indices and other sources over northern Namibia Cuvelai Basin. *Jamba J Disaster Risk Stud.* <https://doi.org/10.4102/jamba.v7i1.177>
- Pipaud I, Loibl D, Lehmkühl F (2015) Evaluation of TanDEM-X elevation data for geomorphological mapping and interpretation in high mountain environments—a case study from SE Tibet China. *Geomorphology* 246:232–254. <https://doi.org/10.1016/j.geomorph.2015.06.025>
- Rizzoli P, Martone M, Gonzalez C, Wecklich C, Borla Tridon D, Bräutigam B, Bachmann B, Schulze D, Fritz T, Huber M, Wessel B, Krieger G, Zink M, Moreira A (2017) Generation and performance assessment of the global TanDEM-X digital elevation model. *ISPRS J Photogram Rem Sens* 132:119–139. <https://doi.org/10.1016/j.isprsjprs.2017.08.008>
- Shifidi VT (2014) Socio-Economic Assessment of the consequences of flooding in Northern Namibia, Thesis (MA) Stellenbosch University (2014–12), p. 248
- Shrivathsa B, Panjwani J (2017) Lane Detection using GPS-PPP and VISUAL Method. *Asian J Appl Sci Technol (AJAST)*. 1(5):137–141
- Skakun S, Kussul N, Shelestov A, Kussul O (2012) Flood hazard and flood risk assessment using a time series of satellite images: a case study in Namibia. *Risk Anal* 34(8):1521–1537. <https://doi.org/10.1111/risa.12156>
- Skog I, Handel P (2009) In-car positioning and navigation technologies—a survey. *IEEE Trans Intell Transport Syst* 10(1):4–21. <https://doi.org/10.1109/TITS.2008.2011712>
- Smith B (2003) Accuracy and resolution of shuttle radar topography mission data. *Geophys Res Lett* 30(9):47. <https://doi.org/10.1029/2002GL016643>
- Teunissen PJG, Khodabandeh A (2014) Review and principles of PPP-RTK methods. *J Geod* 89(3):217–240. <https://doi.org/10.1007/s00190-014-0771-3>
- United Nations Office for the Coordination of Humanitarian Affairs Regional Office for South Africa (2018): https://data.humdata.org/search?ext_subnational=1&ext_geodata=1&group_s=nam&q=&ext_page_size=25desc. Accessed 16 Feb 2018
- Wang L, Li Z, Ge M, Neitzel F, Wang Z, Yuan H (2018) Validation and assessment of multi-GNSS real-time precise point positioning in simulated kinematic mode using IGS real-time service. *Remote Sens* 10:337
- Wendleder A, Wessel B, Roth A, Breunig M, Martin K, Wagenbrenner S (2013) TanDEM-X water indication mask generation and first evaluation results. *IEEE J Sel Top Appl Earth Obs Remote Sens* 6(1):171–179. <https://doi.org/10.1109/JSTARS.2012.2210999>
- Wessel B (2016) TanDEM-X Ground Segment—DEM products specification document, EOC DLR Oberpfaffenhofen Germany Public Document TD-GS-PS-002 Issue 3.1 2016
- Xu H (2012) Application of GPS-RTK Technology in the land change survey. *Procedia Eng* 29:3454–3459. <https://doi.org/10.1016/j.proeng.2012.01.511>
- Zumberge JF, Heflin MB, Jefferson DC, Watkins MM, Webb FH (1997) Precise point positioning for the efficient and robust analysis of GPS data from large networks. *J Geophys Res* 102(B3):5005–5017. <https://doi.org/10.1029/96JB03860>

Publisher's Note Springer Nature remains neutral with regard to jurisdictional claims in published maps and institutional affiliations.